

Article

# Microstructure and Minerals Evolution of Iron Ore Sinter: Influence of SiO<sub>2</sub> and Al<sub>2</sub>O<sub>3</sub>

Zhiyun Ji, Yuanjie Zhao, Min Gan \*, Xiaohui Fan, Xuling Chen and Lin Hu

School of Minerals Processing and Bioengineering, Central South University, No.932, South Lushan Road, Changsha 410083, China

\* Correspondence: csu\_ganmin@csu.edu.cn; Tel.: +86-0731-88877214

Received: 17 June 2019; Accepted: 17 July 2019; Published: 19 July 2019



**Abstract:** SiO<sub>2</sub> and Al<sub>2</sub>O<sub>3</sub> are two important minerals that can affect the mechanical and metallurgical properties of sinter. This investigation systematically studied the influences of these minerals and revealed their functional mechanisms on sinter quality. Results showed that with an increasing Al<sub>2</sub>O<sub>3</sub> content in sinter, the sintering indexes presented an improvement before the content exceeded 1.80%, while the quality decreased obviously after the content exceeded 1.80%. With an increasing SiO<sub>2</sub> content, the sinter quality presented a decreasing tendency, especially when the content exceeded 4.80%. Consequently, the optimal content of Al<sub>2</sub>O<sub>3</sub> was ≤1.80% and that of SiO<sub>2</sub> was ≤4.80%. The evolution of the microstructure and minerals in sinter showed that enhancing the Al<sub>2</sub>O<sub>3</sub> content increased the proportion of SFCA generated, which improved the sinter's mechanical strength, while excessive Al<sub>2</sub>O<sub>3</sub> led to the formation of sheet-like SFCA with weak mechanical strength. Increasing the content of SiO<sub>2</sub> strained the formation of SFCA and promoted the formation of calcium silicate, the mechanical strength of which is lower than that of SFCA. The research findings will be useful in guiding practical sintering processes.

**Keywords:** iron ore sintering; Al<sub>2</sub>O<sub>3</sub> and SiO<sub>2</sub>; mineral evolution; function mechanism

## 1. Introduction

China has been the largest crude steel producers in the world since 1996; it has reached a production level of 0.83 billion tons in 2017 [1]. The huge steel output has made it impossible for the domestic iron ore deposits to meet the demand for iron ores. In fact, a major part of the iron ores consumed rely on imports. Australia, Brazil, Canada, South Africa, etc. are the main iron ore exporters, and the long-term data show that the iron ores imported by China have even exceeded 90% of the iron ores consumed [2].

However, the high utilization of imported iron ores has also given rise to some problems. Iron ores containing a high content of Al<sub>2</sub>O<sub>3</sub> make up relatively higher proportions of those imported, though these have been verified to have adverse effects on the quality and metallurgical properties of sinter [3,4]. Moreover, the SiO<sub>2</sub> content in imported iron ores is relatively lower than that of the domestic iron ore concentrates, which helps to produce sinter with lower impurity levels. However, an excessively low SiO<sub>2</sub> content would lead to insufficient generation of SFCA (Quaternary compound of calcium ferrite containing silicate and alumina) under the same basicity (mass ratio of CaO to SiO<sub>2</sub> in sinter). In short, SiO<sub>2</sub> serves as an important mineral to guarantee the mechanical strength of sinter [5,6]. To address the drawbacks of imported iron ores used for sintering and the subsequent smelting process, much work has been conducted to investigate how the content levels of Al<sub>2</sub>O<sub>3</sub> and SiO<sub>2</sub> affect sintering performance. Still, their influence has not been clearly revealed, and some points were even found to be contradictory. It has been widely regarded that a content of Al<sub>2</sub>O<sub>3</sub> exceeding 2.5% will deteriorate the sinter quality, while the influence of an Al<sub>2</sub>O<sub>3</sub> content ≤2.5% on sinter quality

has not been clearly elucidated [7–10]. The research regarding the influence of SiO<sub>2</sub> content on sinter quality has mainly been conducted by changing the content of CaO in sinter as well, so it is difficult to reveal how only the content of SiO<sub>2</sub> affects the sintering performance [11–14].

In this investigation, the influence of Al<sub>2</sub>O<sub>3</sub> and SiO<sub>2</sub> contents on sintering performance was systematically researched, with typical imported iron ores used to alter the contents of these minerals in the sinter. Moreover, the potential function mechanisms of Al<sub>2</sub>O<sub>3</sub> and SiO<sub>2</sub> were elucidated by revealing the microstructure and mineral evolution, with the help of optical microstructure, SEM-EDS, and mineral hardness testing devices. The research findings will provide theoretical guidance for the production of desirable sinter products under the current situation of limited resources.

## 2. Materials and Methods

### 2.1. Materials

Typical iron ores, including Brazilian iron ores, Australian iron ores, Indian iron ores, South Africa iron ores, Canadian iron ores, and domestic (Chinese) iron ores, were used in this investigation. They were provided by integrated steelworks, and their chemical compositions are given in Table 1. It was found that the Australian and Indian iron ores were characterized by relatively higher Al<sub>2</sub>O<sub>3</sub> contents, while the domestic iron ores were characterized by higher SiO<sub>2</sub> contents. These iron ores were used in varying proportions to prepare ore blends with different compositions, so that the Fe, SiO<sub>2</sub>, and Al<sub>2</sub>O<sub>3</sub> contents of the sinter could be adjusted over a relatively wide range. Table 2 gives the chemical compositions of other necessary raw materials used to produce the sinter, including limestone, dolomite, quicklime, coke breeze, and return fines.

**Table 1.** Chemical compositions of iron ores.

Iron Ore Types	Number	Chemical Compositions/%						<sup>b</sup> LOI/%
		<sup>a</sup> TFe	FeO	CaO	MgO	SiO <sub>2</sub>	Al <sub>2</sub> O <sub>3</sub>	
Typical Brazilian iron ores	1 <sup>#</sup>	63.86	5.02	0.10	0.11	4.59	1.14	2.79
	2 <sup>#</sup>	65.69	1.01	0.00	0.11	3.91	0.69	1.72
	3 <sup>#</sup>	67.22	0.14	0.07	0.27	1.04	1.00	1.78
	4 <sup>#</sup>	68.09	0.22	0.02	0.26	1.38	0.39	1.07
	5 <sup>#</sup>	66.08	0.33	0.16	0.16	1.75	1.21	1.25
	6 <sup>#</sup>	60.85	0.51	0.12	0.07	8.42	1.82	2.08
Typical Australian iron ores	7 <sup>#</sup>	62.13	2.59	0.33	0.26	3.80	1.93	4.81
	8 <sup>#</sup>	61.79	1.15	0.08	0.26	4.22	1.98	4.88
	9 <sup>#</sup>	61.93	0.86	0.04	0.18	2.93	1.77	6.32
	10 <sup>#</sup>	61.20	0.41	0.08	0.09	3.22	2.51	6.30
	11 <sup>#</sup>	60.19	0.29	0.48	0.20	2.67	1.14	9.08
	12 <sup>#</sup>	57.21	1.29	0.00	0.10	5.62	1.37	11.21
Typical Indian iron ores	13 <sup>#</sup>	63.32	1.72	0.05	0.16	2.84	2.32	3.71
	14 <sup>#</sup>	58.21	0.27	0.09	0.09	5.51	3.49	5.93
	15 <sup>#</sup>	62.80	1.54	0.29	0.34	4.79	2.64	2.19
Typical South Africa iron ores	16 <sup>#</sup>	64.33	0.29	0.19	0.24	4.84	1.60	0.90
	17 <sup>#</sup>	63.06	0.24	0.10	0.04	6.02	2.04	1.38
	18 <sup>#</sup>	65.17	0.29	0.15	0.04	4.26	1.15	0.63
Typical Canadian iron ores	19 <sup>#</sup>	66.8	12.54	0.53	0.80	4.02	0.10	0.34
Typical domestic iron ores	20 <sup>#</sup>	54.84	2.45	0.47	0.31	13.64	1.68	1.05
	21 <sup>#</sup>	63.46	22.42	1.19	0.82	5.97	0.89	1.61
	22 <sup>#</sup>	60.07	18.11	1.33	0.93	7.00	2.16	3.02
	23 <sup>#</sup>	62.89	21.27	0.09	0.38	9.68	0.84	1.40

<sup>a</sup> TFe = total iron contents; <sup>b</sup> LOI = loss on ignition in air at 950 °C.

**Table 2.** Chemical composition of flux, fuel, and return fines.

Material Types	Chemical Composition							LOI/%
	TFe	FeO	CaO	MgO	SiO <sub>2</sub>	Al <sub>2</sub> O <sub>3</sub>	S	
Limestone	-	-	50.66	2.28	1.49	-	-	40.72
Dolomite	-	-	32.64	19.83	0.71	-	-	46.47
Quicklime	-	-	75.33	3.60	3.58	-	0.17	17.03
Coke breeze	4.11	-	1.54	0.28	2.63	1.88	-	89.16
Return fines	55.46	10.21	9.42	2.02	5.03	4.30	0.58	0.21

## 2.2. Methods

### 2.2.1. Sinter Pot Trials

A cylindrical laboratory-scale sinter pot (700 mm in height and 180 mm in diameter) was used to conduct the sinter pot trials. The raw materials, including iron ores, fluxes, solid fuels, and return fines, first underwent a mixing process. Water was added at the same time to wet the mixtures; the targeted moisture was 7.5–8.0%. After that, a granulator (1400 mm in length and 600 mm in diameter) was used to granulate the iron ores into bigger granules, with a size range of 3–8 mm, during which the revolving speed was 15 rpm and the duration time was 4 min. One kilogram of sinter with a size range of 10–16 mm was used to form a hearth layer in advance, and then the granulated mixture was used to fill the whole sinter pot. After that, the coke breeze distributed in the surface layer was ignited using a natural gas fueled igniter, with the ignition temperature of  $1050 \pm 50$  °C, ignition time of 1 min, and pressure drop of 5 kPa. The combustion front could then move downward, sustained by an induced draft fan.

The return fines balance (RFB), which is the ratio of the mass of produced return fines to the mass of afforded return fines, was taken as an important indicator to validate the tests of typical sintering indexes, including sintering speed. Productivity is the sinter output per unit area and unit time,  $t \cdot m^{-2} \cdot h^{-1}$ . The tumbler index is an important factor to determine the mechanical strength of the sinter based on the methodology outlined in ISO3271 (2007), measured in mass %. However, 15 kg sinter within 10–40 mm is difficult to obtain in laboratory-scale sintering trials. To achieve an effective tumbler index, the width of the tumbler is typically reduced to half or one-fifth. In our investigation, the width of the tumbler was reduced by half, and the standard weight was reduced to 7.5 kg for tumbler index testing. More detailed information about these factors can be found elsewhere [15].

### 2.2.2. Minerals Analysis and Mechanical Strength Examination

A mini-sintering test was used to research the liquid generation properties of minerals under a high temperature. A horizontal heating furnace whose temperature and atmosphere could be controlled by a program was adopted to perform the mini-sintering experiment, which is schematically shown in Figure 1.

The mini-sintering method includes ore blending, briquetting, sintering, and cooling. Specifically, fine-grained iron ores within a size range of  $-5$  mm were mixed with fluxes (limestone, quicklime, and dolomite), and then ground to a size under 0.074 mm and compressed into a standard pyrometric cone (20 mm in height and a side length of 5 mm). The MgO content for each sample was kept at 2.0%. The samples in pyrometric cones were settled on a pallet and the pallet was sent into the heating furnace for roasting. During the roasting process, the heat rate was 10 °C/min and the atmosphere was adjusted with the temperature (Figure 2) according to the reactions in the practical sintering process. While being roasted, a group of triangular pyramid shape pictures were taken by a camera every 10 s, and the property of liquid generation could be obtained through image processing software. The liquid phase formation properties included the initial formation temperature, complete formation temperature, average formation velocity of the liquid phase, and the amount of generated phase. Among them, the initial formation temperature ( $T_s$ ) refers to the point at which the sharp corner of the pyrometric

cone begins to round, while the complete formation temperature ( $T_e$ ) refers to the point at which the pyrometric cone becomes completely rounded. The average formation velocity of liquid phase was calculated using Equation (1). The amount of liquid phase ( $\eta$ ) was reflected by the deformation of the pyrometric cone, which was defined as the variance of projection area between 1000 and 1300 °C. The liquid phase content was calculated according to Equation (2). Detailed information can be found elsewhere [16,17].

$$V = 1000/(T_e - T_s), \quad (1)$$

$$\eta = (S_{1000} - S_{1300})/S_{1000} \times 100\%, \quad (2)$$

where  $\eta$  is the amount of liquid phase,  $S_{1300}$  is the area of the pyrometric cone at 1300 °C, and  $S_{1000}$  is the area of the pyrometric cone at 1000 °C.

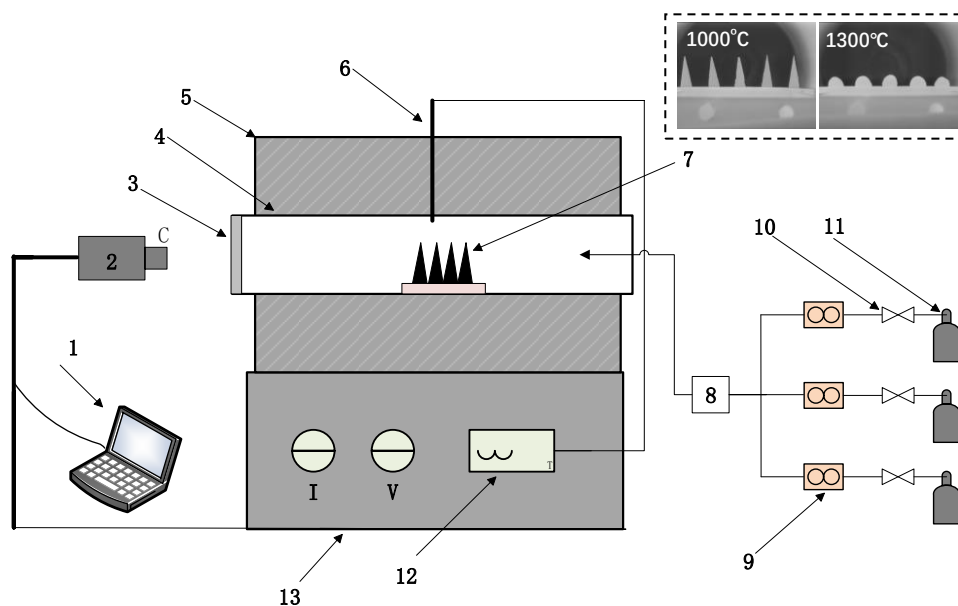


**Figure 1.** The device used for the mini-sintering test. 1—Computer; 2—Camera; 3—Transparent glass; 4—Silicon tube; 5—Heating furnace; 6—Thermocouple; 7—Standard pyrometric cone; 8—Gas mixer; 9—Flowmeter; 10—Reducing valve; 11—Gas bottle; 12—Temperature display panel; 13—Controller.

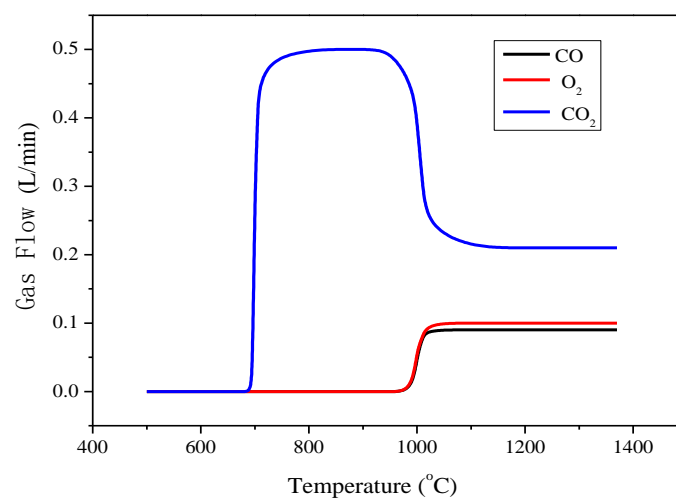


**Figure 2.** Temperature and atmosphere profile during the heating process.

First, 3.5 g iron ore mixture was briquetted into a cylindrical agglomerate under a pressure of 300 kg/cm<sup>2</sup>. After drying, the agglomerate was heated to 1200 °C for 1 h in a high-temperature furnace,

and the whole heating process was conducted in an air atmosphere. The vertical compressive strength of the agglomerate was examined. Subsequently, four parallel tests were conducted, the average value of which was regarded as its compressive strength, N/P (Newton per pellets). An optical microscope, model Leica DMRXE, was used to analyze the microstructure and mineral distribution of the heated agglomerate. Leica Qwin V3 software was used to analyze the compositions of typical minerals according to their special color.

Two important micromechanical factors—fracture toughness and Vickers hardness—were employed to evaluate the mechanical strength-related properties of the sinter. A micro-hardness tester FM-700 (F-T Corporation, Japan) was used to examine the Vickers hardness of typical minerals in the sinter.

### 3. Results and Discussion

#### 3.1. Influences of $Al_2O_3$ and $SiO_2$ on Sintering Performance

Figure 3 shows the influence of  $Al_2O_3$  content on sinter quality, where the content of  $SiO_2$  was around 4.80%, the basicity ( $CaO/SiO_2$ , mass ratio) was 2.0, and the content of  $MgO$  was 2.00%. The permeability of each sintering bed was kept at a similar level with the optimization of the granulation process to avoid the influence of permeability affecting sinter quality. It was found that when the content of  $Al_2O_3$  increased from 1.0 to 1.80%, the tumbler index and productivity changed marginally. However, when the content exceeded 1.80%, both the tumbler index and productivity appeared to drop obviously, which implied a weakened sinter quality. This phenomenon indicates that the optimal content of  $Al_2O_3$  in sinter should be within 1.80%.

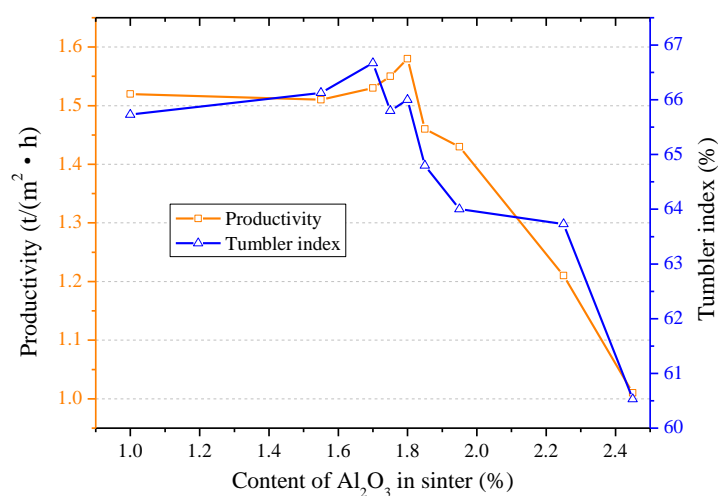


Figure 3. Influence of  $Al_2O_3$  content on productivity and tumbler index.

Figure 4 shows the influence of  $SiO_2$  content on sinter quality, where the content  $CaO$  was around 9.60%, the content of  $MgO$  was 2.00%, and the content of  $Al_2O_3$  was around 1.60%. It was found that when the content of  $SiO_2$  increased from 4.0 to 5.5%, the tumbler index exhibited a continuous drop. In particular, when the content exceeded 4.80%, the tumbler index exhibited a considerable drop from 66.13 to 63.53%. However, when increasing the content further, the tumbler index continued to drop. The productivity remained constant at around  $1.56 t \cdot m^{-2} \cdot h^{-1}$  as the content of  $SiO_2$  increased from 4.00 to 4.80%, but dropped significantly as the content enhanced further. Therefore, the optimal content of  $SiO_2$  should be controlled within 4.80% when the content of  $CaO$  is 9.60%.

#### 3.2. Influences of $Al_2O_3$ and $SiO_2$ on Microcharacteristics of Sinter

Figure 5 shows the influence of the  $Al_2O_3$  content on the microstructure of sinter, revealing that when the content of  $Al_2O_3$  ranged from 1.00% to 2.25%, the distribution area of SFCA showed

an increasing tendency. The statistical data given in Figure 6 shows that the total content of SFCA increased from 37.9 to 52.6% with the content of  $Al_2O_3$  ranged from 1.00 to 2.25%. Moreover, the content of needle-like SFCA increased from 17.2 to 22.3% with the content of  $Al_2O_3$  increasing to 1.80%, and again increased slightly to 22.0% with the content of  $Al_2O_3$  increased to 2.25%. The content of sheet-like SFCA exhibited an obvious enhancement from 11.7 to 22.6%. Additionally, the content of granule-like SFCA changed slightly, within 8.0–11.7%.

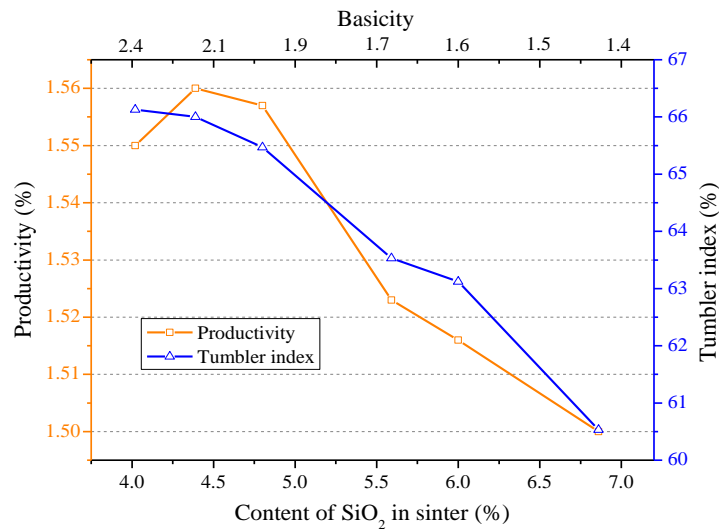


Figure 4. Influence of SiO<sub>2</sub> content on productivity and tumbler index.

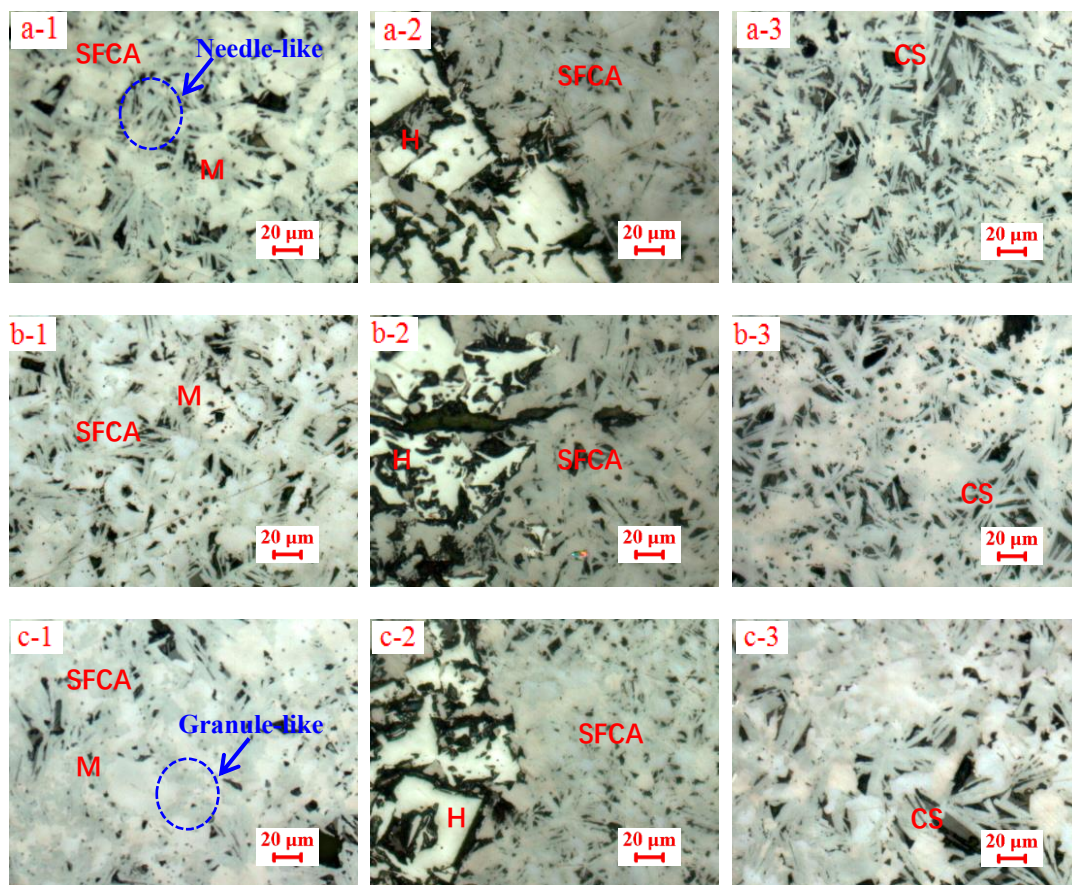
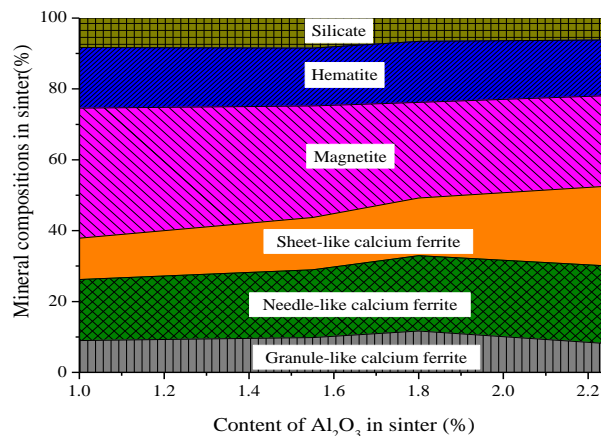


Figure 5. Cont.



**Figure 5.** Effects of  $\text{Al}_2\text{O}_3$  content on microstructure. (a-1,a-2,a-3)  $\text{Al}_2\text{O}_3 = 1.00\%$ ; (b-1,b-2,b-3)  $\text{Al}_2\text{O}_3 = 1.55\%$ ; (c-1,c-2,c-3)  $\text{Al}_2\text{O}_3 = 1.80\%$ ; (d-1,d-2,d-3)  $\text{Al}_2\text{O}_3 = 2.25\%$ ; M—magnetite; H—hematite; CS—silicate.



**Figure 6.** Effects of  $\text{Al}_2\text{O}_3$  content on mineral composition.

Figure 7 shows the influence of the  $\text{SiO}_2$  content on the microstructure of sinter, indicating that with an increasing content of  $\text{SiO}_2$ , the distribution area of SFCA showed a decreasing tendency. From Figure 8 it can be seen that the total content of SFCA dropped from 44.3 to 30.6%. Among the different SFCA varieties, the content of needle-like calcium dropped from 19.7 to 13.2%, the content of sheet-like SFCA dropped from 15.1 to 8.5%. However, the content of silicate increased from 8.4 to 15.3%. Moreover, a large amount of glass phase with low mechanical strength could be observed with an increasing content of  $\text{SiO}_2$ . The SEM-EDS analysis showed that with an increasing content of  $\text{SiO}_2$  (Figure 9 and Table 3), the content of Ca in silicate was increased, which indicated that more Ca was combined with Si. Consequently, this phenomenon resulted in the decrease of Ca to combine with Fe, which served as the reason for the decreased content of SFCA.

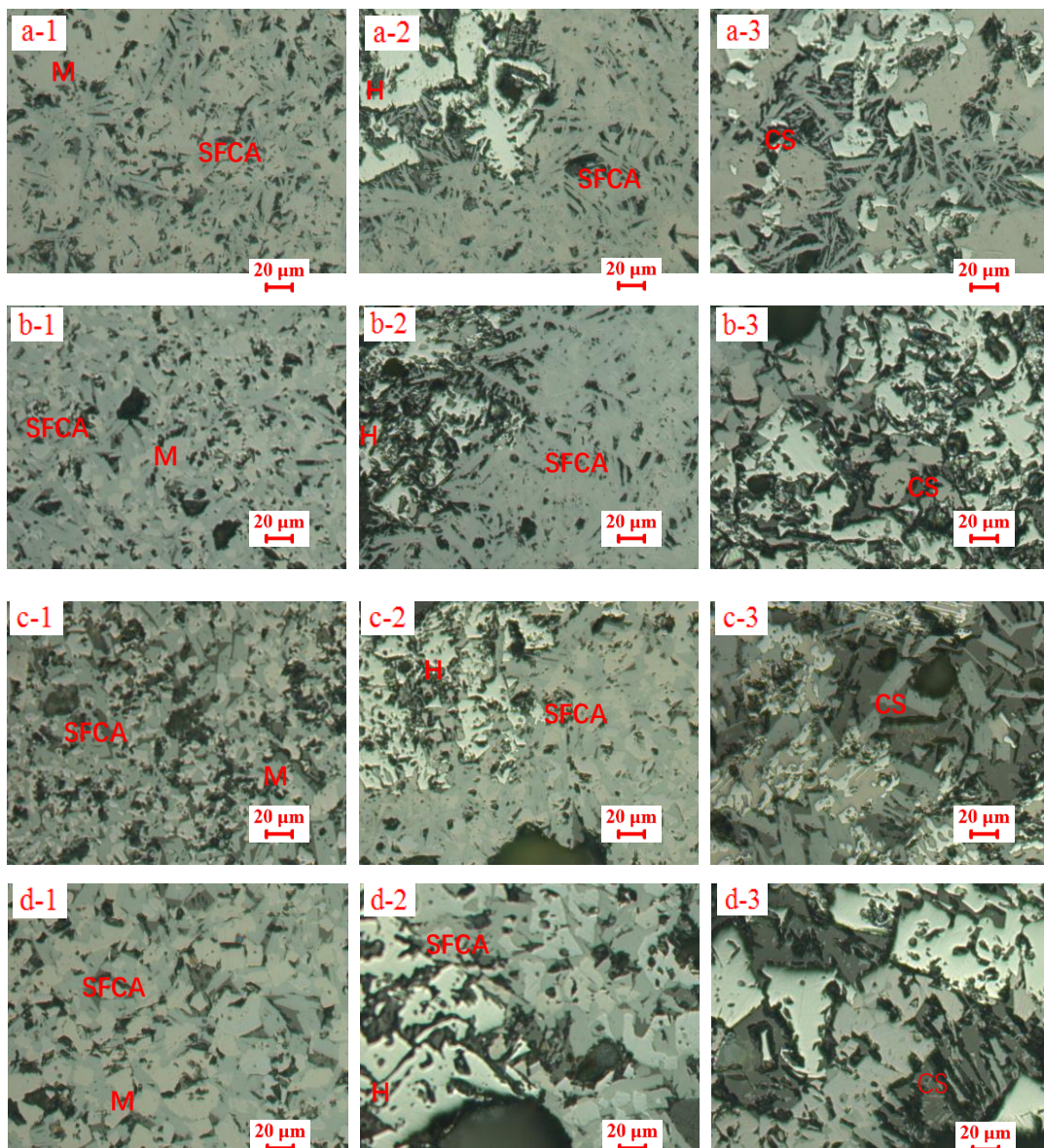


**Figure 7.** Effects of SiO<sub>2</sub> content on microstructure. (a-1,a-2,a-3) SiO<sub>2</sub> = 4.80%; (b-1,b-2,b-3) SiO<sub>2</sub> = 5.32%; (c-1,c-2,c-3) SiO<sub>2</sub> = 5.59%; (d-1,d-2,d-3) SiO<sub>2</sub> = 6.60%; M—magnetite; H—hematite; CS—silicate.

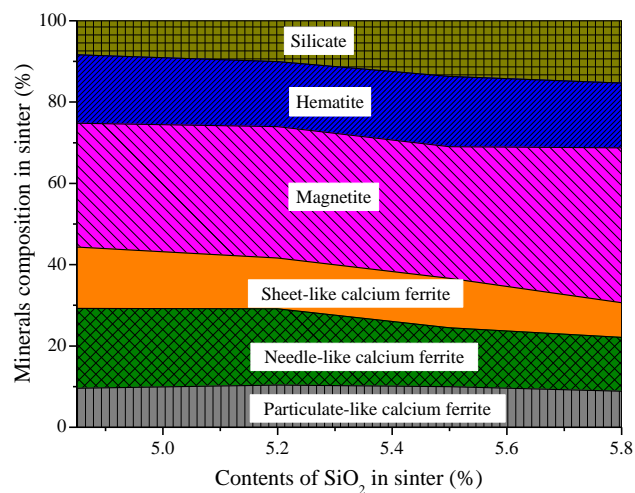


**Figure 8.** Effects of SiO<sub>2</sub> content on mineral composition.

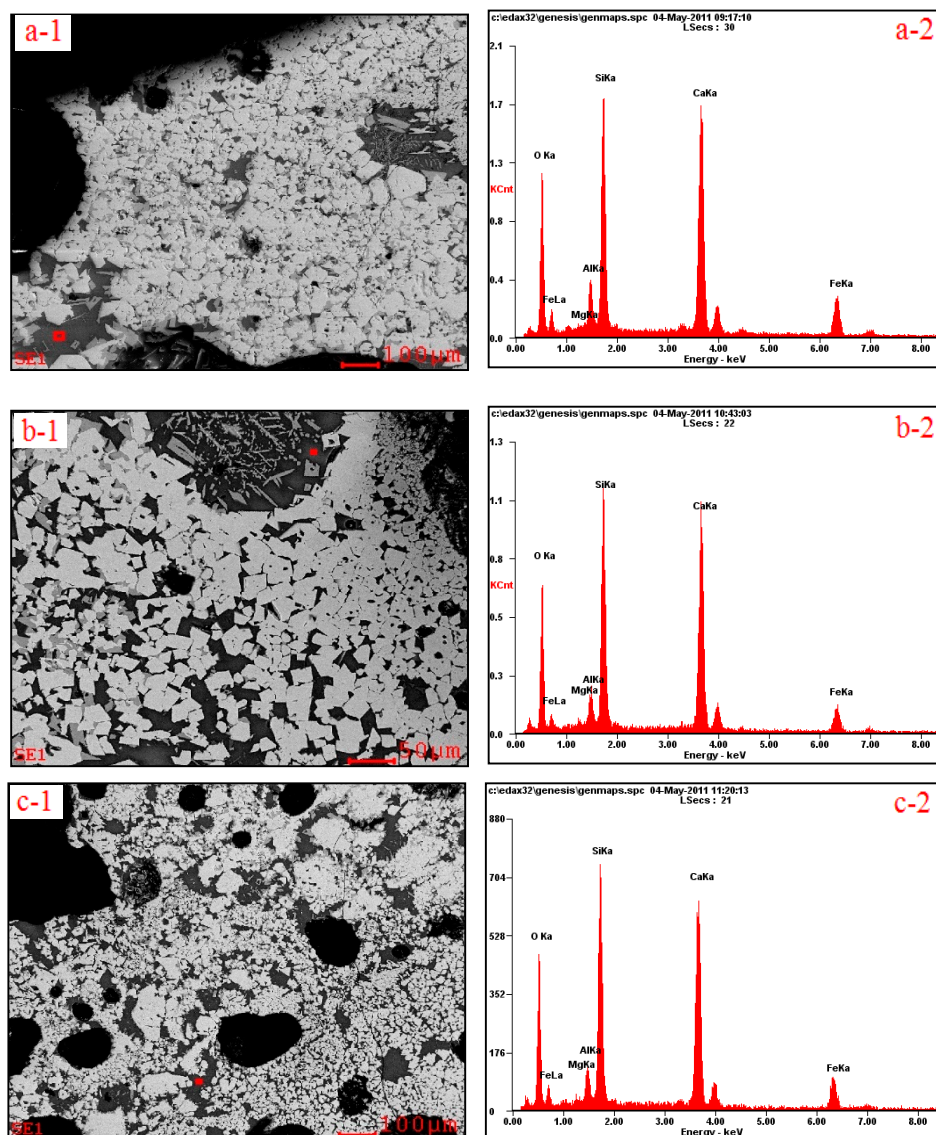


**Figure 9.** SEM-EDS of silicate. (a-1)  $\text{SiO}_2 = 4.00\%$  SEM; (b-1)  $\text{SiO}_2 = 5.32\%$  SEM; (c-1)  $\text{SiO}_2 = 6.00\%$  SEM; (a-2)  $\text{SiO}_2 = 4.00\%$  EDS; (b-2)  $\text{SiO}_2 = 5.32\%$  EDS; (c-2)  $\text{SiO}_2 = 6.00\%$  EDS.

**Table 3.** Effects of  $\text{SiO}_2$  content on composition of silicate.

$\text{SiO}_2/\%$	Ca/%	Si/%	Al/%	Fe/%
4.00	23.44	16.64	2.89	11.39
5.32	26.71	18.15	3.24	9.46
6.00	27.06	18.80	2.52	11.70

### 3.3. Function Mechanisms of $\text{Al}_2\text{O}_3$ and $\text{SiO}_2$ on Sinter Quality

Figure 10 shows the effect of the  $\text{Al}_2\text{O}_3$  content on the formation temperature of the liquid phase, illustrating that with an increasing content of  $\text{Al}_2\text{O}_3$ , the initial generating temperature of the liquid phase and the completely generated temperature exhibited an increasing tendency. Especially when the  $\text{Al}_2\text{O}_3$  content exceeded 1.8%, the temperatures presented an obvious rise. From Figure 11 it can be seen that with an increasing content of  $\text{Al}_2\text{O}_3$ , the amount of formed liquid phase decreased and the average formation speed showed a continuous drop. An obvious drop could also be observed when the content exceeded 1.80%. Therefore, increasing the content of  $\text{Al}_2\text{O}_3$  weakens the liquid phase generation ability.

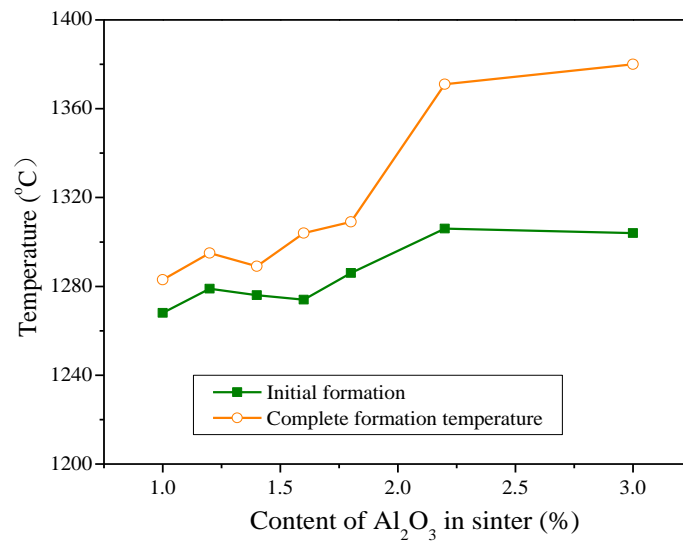


Figure 10. Effects of Al<sub>2</sub>O<sub>3</sub> content on the formation temperature of the liquid phase.

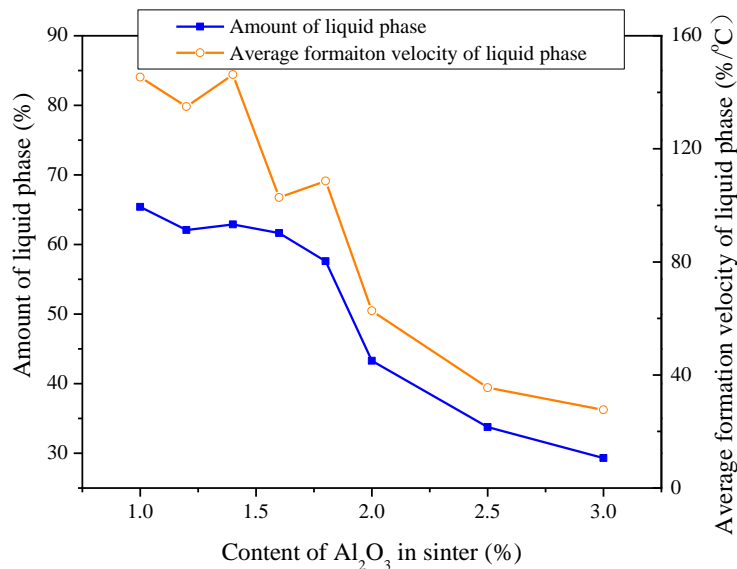
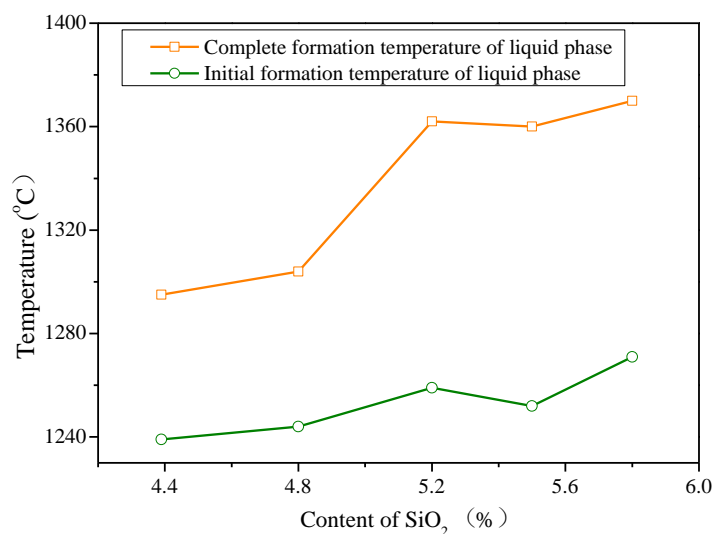
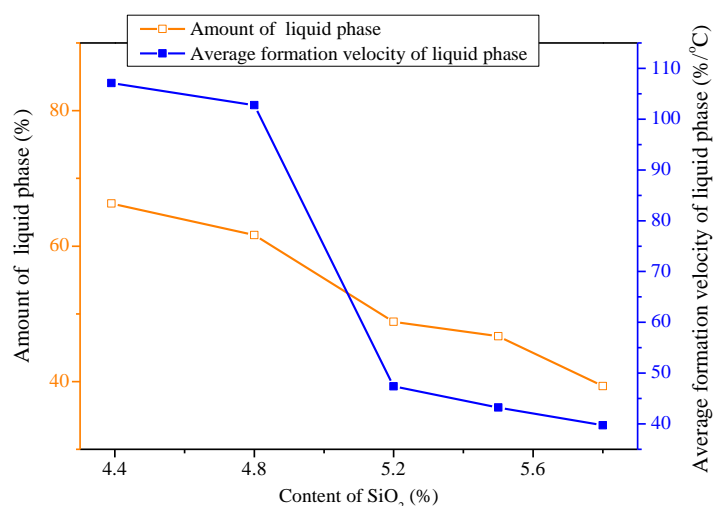


Figure 11. Effects of Al<sub>2</sub>O<sub>3</sub> content on the production and formation rate of the liquid phase.

Figure 12 depicts the influence of the SiO<sub>2</sub> content on the initial liquid phase and complete formation temperatures, showing that with an increasing content of SiO<sub>2</sub>, the temperatures showed an increasing tendency. Moreover, after the content of SiO<sub>2</sub> exceeded 4.80%, the complete formation temperature exhibited an obviously rise. Figure 13 shows the influence of the SiO<sub>2</sub> content on the generation amount and generation speed of the liquid phase. It was found that increasing the content of SiO<sub>2</sub> led to a decrease in these factors. Especially when the content of SiO<sub>2</sub> exceeded 4.80%, an obvious drop was observed.



**Figure 12.** Influence of SiO<sub>2</sub> content on the formation temperature of the liquid phase.



**Figure 13.** Influence of SiO<sub>2</sub> content on the amount and generation velocity of the liquid phase.

Figure 14 shows the relationship between different species of SFCA and the initial and complete formation temperatures of the liquid phase. It was found that the formation of sheet-like SFCA required higher temperatures—the initial and complete formation temperatures were 1291 °C and 1284 °C, respectively. However, the two typical temperatures of needle-like SFCA were 1279 °C and 1248 °C, respectively. This phenomenon indicates that needle-like SFCA corresponds to lower initial and complete formation temperatures. Figure 15 shows the amount of formed liquid phase and the formation speed. It can be seen that the formation of needle-like SFCA corresponded to the rapid formation of the liquid phase.

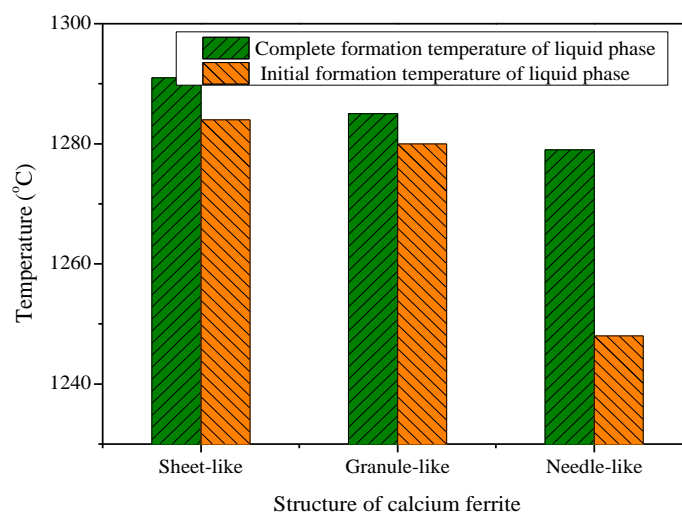


**Figure 14.** Relationship between the structures of SFCA and the liquid formation temperatures of SFCA.

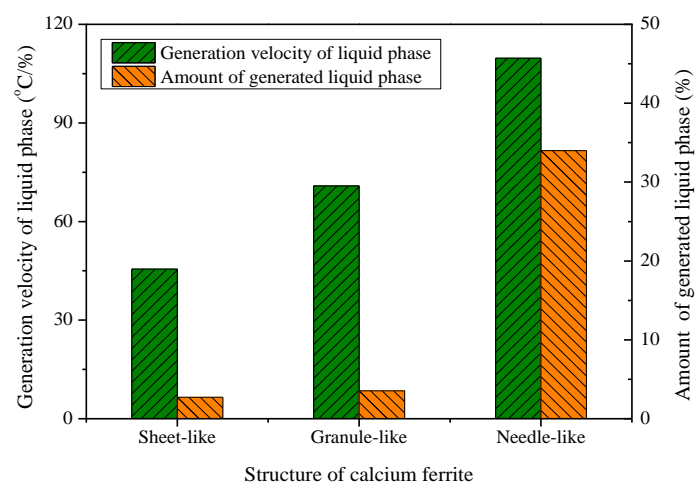


**Figure 15.** Relationship between the structures of SFCA and the liquid formation properties and SFCA.

As stated above, increasing the content of  $\text{Al}_2\text{O}_3$  in sinter promoted the formation of SFCA, with the content of sheet-like SFCA being enhanced to a much extent compared to needle-like SFCA. This could be attributed to the increased formation temperature of the liquid phase and the decreased generation velocity of the liquid phase, which favored the liquid formation properties of sheet-like SFCA, especially when the content of  $\text{Al}_2\text{O}_3$  exceeded the recommended value of 1.80%. Moreover, with an increasing content of  $\text{SiO}_2$ , the amount of SFCA decreased. This also be attributed to its influence on the formation properties of the liquid phase, with the exception of that fact that more Ca was transformed into silicate. A higher content of  $\text{SiO}_2$  in sinter led to a higher formation temperature of SFCA, and the generation velocity of  $\text{SiO}_2$  also presented an obvious drop when the content of  $\text{SiO}_2$  exceeded 4.80%.

To further reveal the effects of  $\text{SiO}_2$  and  $\text{Al}_2\text{O}_3$  on sinter quality, the mechanical strengths of different species of SFCA were examined. As shown in Figure 16, needle-like SFCA showed the highest compression strength of 1809 N, which was considerably higher than that of sheet-like SFCA, which reached 1186 N, and that of the calcium silicate, which showed the lowest compression strength of 1035 N. These results agree well with those of Loo et al. and Ying et al. [18,19]. Moreover, the fracture toughness and Vickers hardness of different kinds of minerals were also measured, and the results are shown in Figure 17. It can be seen that the silicate presented the lowest hardness of 404.38 Gg/m<sup>2</sup> and fracture toughness of 0.524 MN/m<sup>3/2</sup>. Therefore, increasing the content of  $\text{SiO}_2$  in sinter would lead to the decrease of the tumbler index as more silicate is formed. Moreover, among the different SFCA types, needle-like SFCA showed

the highest hardness of 683.31 Gg/m<sup>2</sup> and fracture toughness of 1.30 MN/m<sup>3/2</sup>. Sheet-like SFCA showed a much lower hardness of 489.34 Gg/m<sup>2</sup> and a fracture toughness of 0.65 MN/m<sup>3/2</sup>. As a consequence, it is not hard to understand that increasing the content of Al<sub>2</sub>O<sub>3</sub> would decrease the tumbler index of sinter, as more sheet-like SFCA with lower mechanical strength is formed.

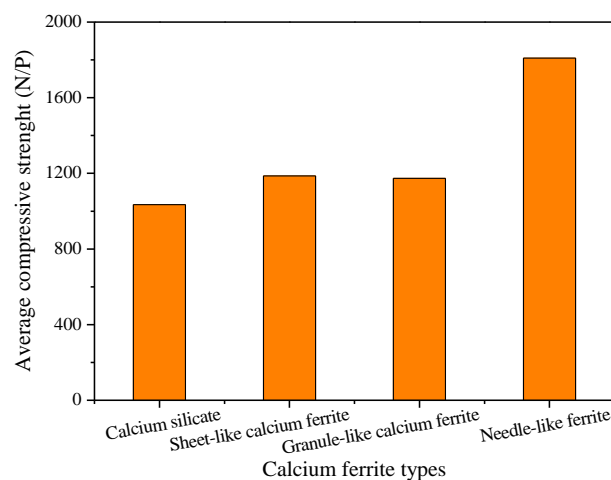


Figure 16. Average compressive strength of typical kinds of minerals.

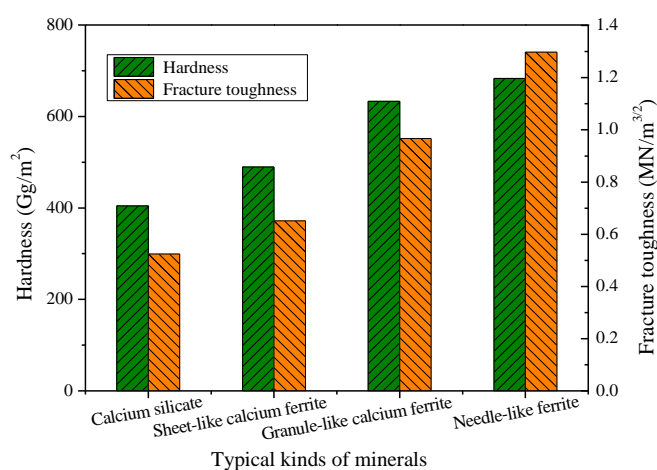


Figure 17. Fracture toughness and Vickers hardness of typical kinds of minerals.

#### 4. Conclusions

(1) The influence of the Al<sub>2</sub>O<sub>3</sub> content on sinter quality was revealed—increasing the content to 1.80% improved the tumbler index and productivity, while an obvious drop occurred when the content exceeded 1.80%. This suggests that the optimal Al<sub>2</sub>O<sub>3</sub> content in sinter should be controlled to be within 1.80%. A potential reason for this result is that the generation amount of bonding phase SFCA increases as the Al<sub>2</sub>O<sub>3</sub> content rises, while sheet-like SFCA with a lower mechanical strength predominates when the content exceeds 1.80%.

(2) The influence of the SiO<sub>2</sub> content on sinter quality was revealed—enhancing the content led to the decrease of the tumbler index, especially when the content exceeded 4.80%, while the average amount of silica in sinter in practical sintering plants ranges between 5 and 5.5%. This result can be attributed to the formation of calcium silicate with lower mechanical strength, which reduces the effective amount of CaO to react with Fe<sub>2</sub>O<sub>3</sub> to form SFCA with a lower mechanical strength.

(3) Our research findings elucidated the effects of changing Al<sub>2</sub>O<sub>3</sub> and SiO<sub>2</sub> contents on sintering performance, which is useful for guiding efficient sinter production processes using large amounts of imported iron ores.

**Author Contributions:** The whole work was done by the authors listed in this paper, specifically, conceptualization, M.G.; methodology, L.H.; software, L.H.; validation, Z.J., M.G., and X.F.; formal analysis, Z.J., X.C., and Y.Z.; investigation, L.H.; resources, X.F.; data curation, L.H.; writing—original draft preparation, Z.J.; writing—review and editing, X.F.; visualization, X.F.; supervision, X.F.; project administration, X.F.; funding acquisition, X.F. and Z.J.

**Funding:** This work was financially supported by the National Natural Science Foundation of China (Grant No. U1660206 and Grant No. 51804347) and the Foundation supported by Central South University for Young Teachers.

**Conflicts of Interest:** The authors declare no conflict of interest.

## References

1. Zhang, Q.; Zhang, W.; Wang, Y.J.; Xu, J.; Cao, X.C. Potential of energy saving and emission reduction and energy efficiency improvement of China's steel industry. *Iron Steel* **2019**, *54*, 7–14.
2. Li, X.C. Road map to high-quality development of iron and steel industry in new age. *Iron Steel* **2019**, *54*, 1–7.
3. Hessien, M.M.; Kashiwaya, Y.; Ishii, K.; Nasr, M.I.; El-Geassy, A.A. Sintering and heating reduction processes of alumina containing iron ore samples. *Ironmak. Steelmak.* **2008**, *35*, 191–204. [[CrossRef](#)]
4. Umadevi, T.; Prakash, S.; Bandopadhyay, U.K. Influence of alumina on iron ore sinter quality and productivity. *World Iron Steel* **2010**, *4*, 12–18.
5. Clout, J.; Manuel, J. Fundamental investigations of differences in bonding mechanisms in iron ore sinter formed from magnetite concentrates and hematite ores. *Powder Technol.* **2003**, *130*, 393–399. [[CrossRef](#)]
6. Chen, C.L.; Lu, L.M.; Jiao, K.X. Thermodynamic modelling of iron ore sintering reactions. *Minerals* **2019**, *9*, 361. [[CrossRef](#)]
7. Park, J.H.; Cho, Y.J.; Yoon, S.S. Effect of Al<sub>2</sub>O<sub>3</sub>, SiO<sub>2</sub> and MgO on the formation of SFCAs in sinter using X-ray diffraction method. *J. Korean Inst. Met. Mater.* **2002**, *40*, 811–817.
8. Liu, J.B.; Li, L.S. Influence of Al<sub>2</sub>O<sub>3</sub> on sinter for its phase compositions and properties in equilibrium. *J. Anhui Univ. Technol.* **2009**, *26*, 333–337.
9. Lu, L.; Holmes, R.J.; Manuel, J.R. Effect of alumina on sinter performance of hematite iron ores. *ISIJ Int.* **2007**, *47*, 349–358. [[CrossRef](#)]
10. Webster, N.A.S.; Odea, D.P.; Ellis, B.G.; Pownceby, M.I. Effects of gibbsite, kaolinite and Al-rich goethite as alumina sources on silico-ferrite of calcium and aluminum (SFCA) and SFCA-I iron ore sinter bonding phase formation. *ISIJ Int.* **2017**, *57*, 41–47. [[CrossRef](#)]
11. Webster, N.A.S.; Pownceby, M.I.; Madsen, I.C.; Studer, A.J.; Manuel, J.R.; Kimpton, J.A. Fundamentals of silico-ferrite of calcium and aluminum (SFCA) and SFCA-I iron ore sinter bonding phase formation: Effects of CaO:SiO<sub>2</sub> ratio. *Metall. Mater. Trans. B* **2014**, *45*, 2097–2105. [[CrossRef](#)]
12. Feng, X.P.; Zhang, Y.Z. Influence of basicity on the low silicon sinter strength. *Sinter. Pelletizing* **2004**, *29*, 41–47.
13. Zhang, Y.Z.; Feng, X.P.; Li, Z.G.; Yin, H.S. Study and practice of improving the metallurgical property of low silicon sinter. *Sinter. Pelletizing* **2004**, *29*, 4–7.
14. Wang, R.C.; Fu, J.Y. Study on production of high Fe and Low SiO<sub>2</sub> Sinter. *Iron Steel* **2007**, *42*, 18–23.
15. Fan, X.H.; Ji, Z.Y.; Gan, M.; Chen, X.L.; Jiang, T. Integrated assessment on the characteristics of straw-based fuels and their effects on iron ore sintering performance. *Fuel Process. Technol.* **2016**, *150*, 1–9. [[CrossRef](#)]
16. Fan, X.H.; Jiang, T.; Gan, M. A Method for Detecting the Liquid Phase Formation Characteristics of Sintered Iron Ore. Chinese Patent ZL200910307772.9, 22 June 2011.
17. Gan, M.; Fan, X.H.; Chen, X.L.; Ji, Z.Y. High temperature mineralization behavior of mixtures during iron ore sintering and optimizing methods. *ISIJ Int.* **2015**, *55*, 742–750. [[CrossRef](#)]
18. Loo, C.E.; Wan, K.T.; Howes, V.R. Mechanical properties of natural and synthetic mineral phases in sinters having varying reduction degradation indices. *Ironmak. Steelmak.* **1998**, *15*, 279–285.
19. Ying, Z.W.; Jiang, M.F.; Xu, L.X. Effects of Mineral Composition and Microstructure on Crack Resistance of Sintered Ore. *J. Iron Steel Res. Int.* **2006**, *13*, 9–12. [[CrossRef](#)]

